Evaluation of [C-11]rofecoxib as PET tracer for cyclooxygenase 2 overexpression in rat models of inflammation

de Vries, Erik F. J.; Doorduin, Janine; Dierckx, Rudi A.; van Waarde, Aren

Published in:
Nuclear Medicine and Biology

DOI:
10.1016/j.nucmedbio.2007.07.015

Publication date:
2008

Available online at www.sciencedirect.com
ScienceDirect
Nuclear Medicine and Biology 35 (2008) 35–42
NUCLEAR MEDICINE — AND — BIOLOGY
www.elsevier.com/locate/nucmedbio

Evaluation of [^{11}C]rofecoxib as PET tracer for cyclooxygenase 2 overexpression in rat models of inflammation

Erik F.J. de Vries*, Janine Doorduin, Rudi A. Dierckx, Aren van Waarde

Department of Nuclear Medicine and Molecular Imaging, University Medical Center Groningen, University of Groningen, P.O. Box 30.001, 9700 RB Groningen, The Netherlands

Received 29 June 2007; received in revised form 27 July 2007; accepted 30 July 2007

Abstract

Background: Overexpression of cyclooxygenase type 2 (COX-2) is triggered by inflammatory stimuli, but it also plays a prominent role in the initiation and progression of various diseases. This study aims to investigate [^{11}C]rofecoxib as a positron emission tomography (PET) tracer for COX-2 expression.

Methods: [^{11}C]Rofecoxib was prepared by methylation of its sulphinate precursor. Regional brain distribution and specific binding of [^{11}C]rofecoxib in healthy rats was studied by ex vivo biodistribution and autoradiography. Regional brain distribution and PET imaging studies were also performed on rats with severe encephalitis, caused by nasal infection with herpes simplex virus (HSV). Finally, ex vivo biodistribution and blocking studies were carried in rats with a sterile inflammation, induced by intramuscular turpentine injection.

Results: [^{11}C]rofecoxib brain uptake in control animals corresponded with the known distribution of COX-2. Pretreatment with NS398 significantly reduced tracer uptake in the cingulate/frontopolar cortex, whereas the reduction in hippocampus approached significance. Ex vivo autoradiography also revealed preferential tracer uptake in hippocampus and cortical areas that could be blocked by NS398. In HSV-infected animals, [^{11}C]rofecoxib uptake was moderately increased in all brain regions, but it could not be blocked with indomethacin. Yet, some PET images revealed increased tracer uptake in brain areas with microglia activation. In turpentine-injected animals, [^{11}C]rofecoxib uptake in inflamed muscle was not higher than in control muscle and could not be blocked with NS398. Indomethacin caused a slight reduction in muscle uptake.

Conclusions: Despite the apparent correlation between [^{11}C]rofecoxib uptake and COX-2 distribution in healthy rats, [^{11}C]rofecoxib could not unambiguously detect COX-2 overexpression in two rat models of inflammation.

Keywords: Positron Emission Tomography; COX-2 inhibitor; NSAID; Inflammation; Microglia activation; Imaging

1. Introduction

Cyclooxygenases (COX) catalyze the first two steps in the conversion of arachidonic acid to prostaglandins and thromboxanes. Thus far, three subtypes of COX have been identified. The inducible subtype of the enzyme, COX-2, plays an important role in the physiological response to inflammatory stimuli. In addition to its role in inflammatory disorders, COX-2 is also implicated in a variety of other pathologies, such as cancer, cardiac and cerebral ischemia, Alzheimer's disease and Parkinson's disease [1]. Under normal physiological conditions, COX-2 is virtually absent in most tissues, except for the constitutive expression in the kidneys and low expression levels in the brain. In the kidney, COX-2 has an important function in the regulation of renal hemodynamics and salt and water homeostasis. The function of COX-2 in the brain is still unknown.

Inflammatory stimuli induce a strong increase in the expression of COX-2. In the brain, the COX-2 overexpression is predominantly located in activated microglia and astrocytes [2]. Overexpression of COX-2 is also observed in the process of neurodegeneration. Patients with stroke or neurodegenerative diseases, like Alzheimer's disease or Parkinson's disease, expressed elevated levels of COX-2 in the affected brain areas [3]. A major problem with studying COX-2 in the human brain is the fact that the

* Corresponding author. Tel.: +31 50 3613311; fax: +31 50 3611687.
E-mail address: e.f.j.de.vries@ngmb.umcg.nl (E.F.J. de Vries).

0969-8051/$ – see front matter © 2008 Elsevier Inc. All rights reserved.
doi:10.1016/j.nucmedbio.2007.07.015

expression levels of the enzyme can only be assessed postmortem by ex vivo laboratory analysis of tissue samples. However, the postmortem analysis of COX-2 is complicated by the instability of COX-2 mRNA and protein (half-life: 1–3.5 h), causing a strong dependence of the results on the interval between analysis and the time of death [4,5]. To overcome this problem, a noninvasive imaging method to monitor COX-2 expression, like positron emission tomography (PET) in combination with a suitable tracer, could be useful. Especially in brain disorders where repetitive tissue sampling is not possible, PET could offer the unique opportunity to gain valuable temporal and spatial information on the expression of COX-2 during disease progression and could thus provide more insight in the role of COX-2 in diseases [6]. In addition, PET imaging could allow in vivo measurement of the occupancy of COX-2 binding sites and, thus, be applied as a surrogate marker for evaluating the efficacy of anti-inflammatory therapy with selective COX-2 inhibitors. This information can be of great value, because in general, it is difficult to correctly predict the behavior of COX-inhibitors in living subjects from in vitro data [7].

In search for a suitable PET tracer for COX-2 imaging, several selective COX-2 inhibitors have been labeled, including [^{18}F]SC58125, [^{18}F]desbromo-DuP-697, [^{11}C]etoricoxib, [^{11}C]celecoxib and [^{11}C]rofecoxib [8–12]. The celecoxib analogue [^{18}F]SC58125 selectively accumulated in COX-2 expressing activated macrophages in vitro but did not show any specific binding to COX-2 in healthy rats or a baboon [8]. [^{18}F]Desbromo-DuP-697 appeared to display COX-2-related specific uptake in rats [9], but a PET study in pigs did not show any specific binding (personal communication). So far, no in vivo evaluation studies of the other radiolabeled COX-2 inhibitors as PET tracers have been published.

Rofecoxib is a highly selective COX-2 inhibitor that has been on the market since 1999 but was withdrawn by the manufacturer in 2004 when a clinical trial showed an increased cardiovascular risk after daily use of 25 mg of the drug for 36 months. Nevertheless, rofecoxib could still be applicable as a PET tracer, since adverse effects are not to be expected after a single injection of a tracer dose of the drug. Moreover, the properties of rofecoxib appear to be in accordance with those of a good PET tracer. Rofecoxib is among the most potent and selective inhibitors of COX-2, with the IC_{50} for COX-2 varying from 18 to 44.6 nM in various cellular assays and with an IC_{50} for COX-1 of >50 μM [13]. In an in vitro human whole blood assay, the COX-1/COX-2 selectivity ratio of rofecoxib was 35.5, which is higher than for other commonly used COX-2 inhibitors. The lipophilicity of rofecoxib should allow penetration of the blood–brain barrier. Ex vivo biodistribution studies in rats revealed that [^{14}C]rofecoxib was distributed rapidly to most tissues within 5 min after intravenous injection and was subsequently washed out [14]. The major elimination route of rofecoxib is by hepatic metabolism with subsequent excretion of the metabolites into the urine. The metabolites of rofecoxib are inactive as COX-2 inhibitors. Recently, the labeling of rofecoxib with carbon-11 was described by Majo et al. [10], but no evaluation of this compound has been reported yet. In this study, we describe an alternative labeling strategy for [^{11}C]rofecoxib (Fig. 1) and the evaluation of this tracer in healthy rats and two distinct rat models of inflammation.

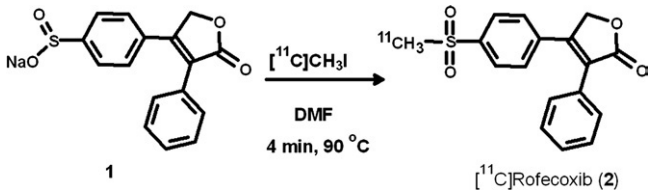

Fig. 1. Radiosynthesis of [^{11}C]rofecoxib via alkylation of the sulphinate precursor with [^{11}C]methyl iodide.

2. Materials and methods

2.1. Materials

Solvents and reagents were obtained from commercial suppliers and used without further purification. High-performance liquid chromatography (HPLC) analyses and preparative separations were performed on a Waters system, consisting of a 515-isocratic pump, a 486-multiwavelength UV detector operated at 274 nm and a Bicron Geiger–Müller radioactivity detector.

2.2. Sulfinate precursor (1)

Sulfinate precursor **1** was received as a kind gift from a company that synthesized the compound from rofecoxib according to the following general method. Methyl sulfone (rofecoxib, 1.0 mmol) was dissolved in 15 ml of tetrahydrofuran (THF) and cooled in ice. A solution of 3 M methyl magnesium chloride (4.5 mmol) in THF was added and the mixture stirred at ambient temperature for 1 h. When HPLC showed remaining starting material, a further aliquot of Grignard reagent (1.5 mmol) was added. After stirring for another 30 min, a solution of tri-*n*-butylborane in THF (6 mmol) was added, and the mixture was heated at reflux until reaction was complete (approximately 11 h). The mixture was poured into 250 ml of diethyl ether, and the precipitate was filtered. The precipitate was dissolved in THF/water (2/1) and aqueous sodium carbonate was added until the pH was ~12. The precipitated magnesium salts were filtered and the filtrate evaporated to dryness. The crude product was purified by reverse phase chromatography (C18, 10 g). The crude product was introduced onto the column (preequilibrated in water) in water containing ~5% methanol and eluted with a gradient of water rising to methanol/water 1/4. The appropriate fractions were

combined and evaporated to dryness giving the required sodium sulfinate.

2.3. Labeling of [^{11}C]Rofecoxib

[^{11}C]Methane was produced via the $^{14}N(p,\alpha)^{11}C$ nuclear reaction by irradiating the N_2+5% H_2 target gas with 17 MeV protons using a Scanditronix MC17 cyclotron. [^{11}C]Methyl iodide was prepared from [^{11}C]methane via procedures that were previously described in the literature [15]. [^{11}C]Methyl iodide was transported by a stream of argon (20 ml/min) into a minivial containing 1 mg sulfinate precursor **1** in 300 μl N,N-dimethylformamide (DMF) at room temperature. After the trapping of [^{11}C]methyl iodide was complete, the reaction mixture was heated at 90°C for 4 min. The reaction mixture was diluted with 1.5 ml water and injected into a semipreparative reversed-phase SymmetryPrep C18 HPLC column (7 μm, 7.8×300 mm). Purification of the product was accomplished with 35% aqueous ethanol as the eluent at a flow rate of 3 ml/min. The radioactive product with a retention time of 10 min was collected (retention time of the precursor: 4 min). The product was diluted with sterile and pyrogen-free water until the ethanol concentration was ≤10% (v/v). The identity of the product was confirmed by coinjection with an authentic sample on reversed-phase HPLC. The radiochemical purity of the product was determined by analytical reversed phase HPLC using an Alphabond C18 column (10 μm, 3.9×300 mm) and 30% acetonitrile in water as the eluent at a flow rate of 1.5 ml/min (retention time: 8 min).

2.4. Animals

All animal studies were carried out in compliance with the national law on animal experiments. The protocols were approved by the animal ethics committee of the University of Groningen. Healthy male Wistar rats were purchased from Harlan (Horst, the Netherlands). The rats were housed in groups under a 12-hour light–dark regimen at a constant temperature (21°C±2°C). Standard laboratory chow (RMH-B, Hope Farms, the Netherlands) and water were available ad libitum. After arrival, the rats were allowed to acclimatize for at least 7 days.

2.5. Regional brain distribution in healthy rats

Male Wistar rats (287±35 g) rats were anesthetized by ip injection of a mixture of ketamine (25 mg/kg) and medetomidine (0.2 mg/kg). The rats were injected into the tail vein with 36±9 MBq [^{11}C]rofecoxib in approximately 0.4 ml 10% aqueous ethanol. Three groups of animals were investigated. The first group consisted of untreated control animals (n=7). Groups 2 and 3 were iv injected with 1.5 mg/kg of the COX-2 selective inhibitor NS398, either 5 (n=4) or 60 min (n=5) before injection of the tracer, respectively. After 60 min of tracer distribution, the animals were terminated, the brains were excised, dissected in specific regions and weighed. Tracer uptake in the brain tissues was measured using a gamma counter and expressed as standardized uptake value (SUV), which was defined as:

$$SUV = \frac{Tissue\ Activity\ Concentration\left(\frac{MBq}{g}\right) * Body\ Weight(g)}{Injected\ Dose\ (MBq)}$$

2.6. Phosphor storage imaging of brain slices

Sixty min after tail vein injection of [^{11}C]rofecoxib, the brains were excised and frozen in liquid nitrogen. The frozen brain samples were cut into 80-μm-thick slices using a microtome at −6 °C. Brain slices were placed on slides and covered with a multipurpose Cyclone Storage Phosphor Screen (Packard Instruments, Meriden, CT, USA). After exposure for 24 h, the phosphor screens were scanned using a Cyclone imaging system (Packard Instruments).

2.7. Herpes simplex virus encephalitis model

[^{11}C]Rofecoxib was evaluated in the herpes simplex virus (HSV) encephalitis model [16]. At Day 0, viral encephalitis was induced in male Wistar rats by intranasal application of 10^7 plaque-forming units of HSV type 1 in 100 μl phosphate-buffered saline (PBS) (n=5). Controls were treated identically using PBS without virus (n=7). At Day 6 or 7 (depending on the severity of the symptoms), the rats were anaesthetized with a mixture of ketamine (25 mg/kg) and medetomidine (0.2 mg/kg) and iv injected with 54±4 MBq [^{11}C]rofecoxib. A PET scan (microPET Focus 220) was acquired for 60 min. Then, the animals were terminated, and the brain was excised and dissected into separate brain regions. Tissues were weighed, and radioactivity was measured in a gamma counter. In blocking experiments, the nonselective COX inhibitor indomethacin (2.5 mg/kg) was iv injected 5 min before injection of the tracer (n=4).

2.8. Sterile inflammation model

As an animal model of sterile inflammation, male Wistar rats were anesthetized with a 3% isoflurane air mixture and im injected with 0.1 ml turpentine into the thigh of the left hind leg. The animals were divided in three groups: untreated controls (n=4) and rats that were pretreated with either the selective COX-2 inhibitor NS398 (n=3) or the nonselective COX inhibitor indomethacin (n=4). After 24 h, the animals were anesthetized with 3% isoflurane/air. In the pretreated groups, the specific binding sites were saturated by injection of 1.5 mg/kg of COX inhibitor into the tail vein 5 min before administration of 56±16 MBq [^{11}C]rofecoxib. Controls were only injected with the tracer solution. After 60 min of tracer distribution, the animals were terminated by extirpation of the heart while under deep narcosis. The relevant tissues were excised, weighed and measured for radioactivity. Tracer uptake was expressed as SUV.

2.9. Statistical analysis

Tracer uptake values were statistically analyzed using the unpaired two-sided Student's *t* test. Differences between groups were considered statistically significant at $P<05$.

3. Results

3.1. Labeling of [^{11}C]Rofecoxib

[^{11}C]Rofecoxib (**2**) was prepared by methylation of its sulfinate precursor **1** with [^{11}C]methyl iodide (Fig. 1). The decay-corrected radiochemical yield was 57±9% (based on [^{11}C]methyl iodide, n=23). The product was isolated with a specific activity of 14±8 GBq/μmol and a radiochemical purity >99%. For animal studies, the product was formulated in 10% ethanol (v/v) by dilution of the collected HPLC fraction with sterile and pyrogen-free water. The total synthesis time, including preparation of [^{11}C]methyl iodide, HPLC purification and formulation, was approximately 40 min.

3.2. [^{11}C]rofecoxib distribution in healthy rat brain

As the brain is one of the few organs that constitutively expresses COX-2, the regional distribution of [^{11}C]rofecoxib in this organ was determined. Ex vivo brain distribution studies in untreated animals showed a heterogeneous pattern of [^{11}C]rofecoxib accumulation (Table 1), with an average SUV in the total brain of 0.26±0.09. Tracer uptake in cingulate/frontopolar cortex (+34%), hippocampus (+15%), frontal cortex (+11%) and parietal/temporal/occipital cortex (+10%) were significantly higher than average brain uptake, whereas tracer uptake in cerebellum (−16%) and bulbus olfactorius (−12%) were significantly lower (two-sided paired Student's *t* test, $P<.01$). To investigate whether the accumulation of [^{11}C]rofecoxib in the brain was due to specific binding to COX-2, blocking experiments with the selective COX-2 inhibitors NS398 were carried out. When 1.5 mg/kg of NS398 was administered 5 min prior to [^{11}C]rofecoxib injection, the tracer was more homogeneously distributed throughout the brain than in control animals. This NS398-induced change in distribution pattern was accompanied by a significant reduction ($P<.01$) in [^{11}C]rofecoxib accumulation in cingulate/frontopolar cortex (−41%, P=.01), whereas the reduction in hippocampus almost reached significance (−33%, P=.06). These brain regions are known to express significant basal levels of COX-2 in healthy animals [17,18]. Prolongation of the interval between NS398 administration and tracer injection from 5 to 60 min did not result in a significantly greater blockade of tracer binding, indicating that NS398 binding to COX-2 is virtually complete within 5 min.

To confirm the results of the ex vivo biodistribution study, phosphor storage images were obtained from brain sections of untreated healthy rats. Phosphor storage imaging revealed relatively high uptake of [^{11}C]rofecoxib in hippocampus and cortical areas (Fig. 2). This distribution corresponds well with the results of the ex vivo biodistribution and the previously reported basal distribution of COX-2 in the brain

Table 1
Distribution of radioactivity in various brain regions, 60 min after injection of [^{11}C]rofecoxib in Wistar rats

	Control (n=7)	NS398, 5 min (n=4)	NS398, 60 min (n=5)
Amygdala/piriform cortex	0.27±0.09	0.18±0.04	0.20±0.05
Bulbus olfactorius	0.23±0.09	0.20±0.06	0.19±0.05
Cerebellum	0.22±0.08	0.18±0.05	0.21±0.05
Cingulate/frontopolar cortex	0.35±0.11	0.18±0.04 *	0.19±0.04 *
Entorhinal cortex	0.26±0.09	0.18±0.07	0.19±0.03
Frontal cortex	0.29±0.10	0.18±0.07	0.19±0.05
Hippocampus	0.30±0.11	0.17±0.05	0.20±0.04
Medulla	0.28±0.11	0.23±0.08	0.24±0.06
Parietal/temporal/occipital cortex	0.29±0.10	0.20±0.04	0.21±0.05
Pons	0.25±0.08	0.21±0.05	0.22±0.05
Striatum	0.25±0.08	0.19±0.07	0.21±0.06

The COX-2 inhibitor NS398 was iv injected 5 or 60 min before the tracer was administered. Tissue uptake is expressed as SUV±S.D.

* Significantly different from controls, as determined by the Student's *t* test ($P<.05$).

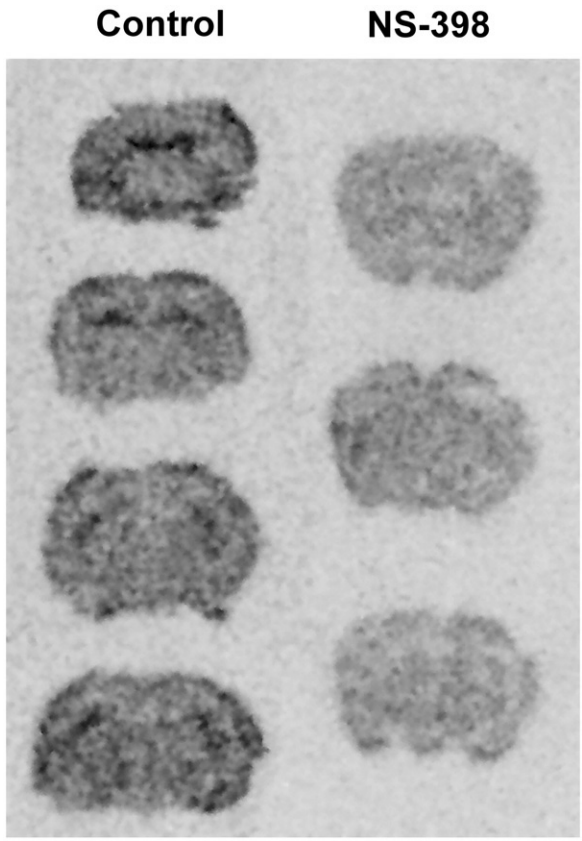

Fig. 2. [^{11}C]Rofecoxib phosphor storage images of coronal brain slices of healthy rats (left), showing selective tracer uptake the hippocampus and cortical areas, and phosphor storage images of the corresponding slices of rats that were pretreated with 1.5 mg/kg NS398 (right).

Table 2
Distribution of radioactivity in various brain regions 60 min after injection of [^{11}C]rofecoxib in control animals and Wistar rats that were intranasally infected with HSV-1

	Control (n=7)	HSV-infected (n=5)	HSV-infected+ indomethacin (n=4)
Amygdala/piriform cortex	0.27±0.09	0.41±0.21	0.53±0.33
Bulbus olfactorius	0.23±0.09	0.31±0.07	0.28±0.04
Cerebellum	0.22±0.08	0.25±0.04	0.23±0.03
Cingulate/frontopolar cortex	0.35±0.11	0.49±0.27	0.55±0.36
Entorhinal cortex	0.26±0.09	0.35±0.14	0.45±0.20
Frontal cortex	0.29±0.10	0.46±0.30	0.36±0.13
Hippocampus	0.30±0.11	0.48±0.30	0.66±0.41
Medulla	0.28±0.11	0.29±0.06	0.26±0.06
Parietal/temporal/occipital cortex	0.29±0.10	0.34±0.10	0.34±0.11
Pons	0.25±0.08	0.29±0.05	0.25±0.04
Striatum	0.25±0.08	0.28±0.06	0.31±0.06

In a subset of infected rats, the COX inhibitor indomethacin was iv injected 5 min before the tracer was administered. Tissue uptake is expressed as SUV±S.D.

[17,18]. When the animals were treated with 1.5 mg/kg NS398 before injection of the tracer, the increased [^{11}C]rofecoxib uptake in hippocampus and cortical areas were reduced to background levels (Fig. 2). Thus, [^{11}C]rofecoxib appears to bind specifically to COX-2 in specific brain regions with highest expression levels of the enzyme.

3.3. [^{11}C]rofecoxib distribution in the Herpes Simplex Virus encephalitis model

Ex vivo biodistribution showed a moderate increase (5–58%) in [^{11}C]rofecoxib uptake in all brain regions of HSV-infected animals, as compared to healthy controls (Table 2), but this increase was not statistically significant for any region (P≥.14). Administration of 2.5 mg/kg of indomethacin to the infected animals did not significantly reduce [^{11}C]rofecoxib uptake in any brain region, indicating the tracer uptake is not saturable.

In accordance to the results of the ex vivo biodistribution study, [^{11}C]rofecoxib microPET images displayed low and rather homogeneous tracer uptake in the brains of HSV-infected animals. In some infected animals, however, slightly higher tracer uptake was observed in the cerebellum and brain stem region. As shown in Fig. 3, areas with increased [^{11}C]rofecoxib uptake corresponded with brain regions that showed enhanced levels of activated microglia, as was determined by [11C]PK11195 PET in a parallel study [19].

3.4. [^{11}C]rofecoxib distribution in a sterile inflammation rat model

Twenty-four hours after injection of turpentine in a thigh muscle of Wistar rats, a sterile inflammation is formed that is characterized by visible swelling of the muscle. Despite the avid inflammatory reaction, ex vivo biodistribution showed that [^{11}C]rofecoxib uptake was not higher in the inflamed muscle than in the contralateral control muscle (Fig. 4). Administration of the selective COX-2 inhibitor NS398 did not significantly affect tracer uptake in the inflamed muscle, control muscle or whole blood. In contrast, treatment with the nonselective COX inhibitor indomethacin caused a significant reduction (P<.05) in tracer uptake in whole blood (−13%) and control muscle (−19%), whereas the reduction in the inflamed muscle approached statistical significance (−15%, P=.09).

4. Discussion

In this study, we investigated the radiolabeled selective inhibitor [^{11}C]rofecoxib as a potential PET tracer for imaging of COX-2 expression. The labeling of [^{11}C]rofecoxib and other COX-2 inhibitors was recently described by Majo et al. [10]. They prepared [^{11}C]rofecoxib from its thiobutyrate ester via a two-step in situ deprotection/methylation–oxidation procedure in 20% radiochemical yield. Here, we described a different labeling strategy starting from the sulphinate precursor of [^{11}C]rofecoxib (**1**). This approach yields [^{11}C]rofecoxib in a single methylation step and gives a radiochemical yield of almost 60%, which is more than sufficient for imaging studies in animals and humans.

To assess the feasibility of [^{11}C]rofecoxib as a PET tracer for COX-2, the brain uptake of this compound was evaluated in healthy Wistar rats, as the brain is one of the few tissues with constitutive COX-2 expression, although expression levels are low under normal conditions. By an ex vivo COX peroxidase assay, we have previously confirmed that the brain is among the organs with highest COX enzyme activity [9]. Pharmacokinetic studies have shown that rofecoxib rapidly penetrates the brain, resulting in cerebrospinal fluid concentrations that are more than fivefold higher than for other COX-2 inhibitors, like celecoxib and valdecoxib [20]. This difference was ascribed to the smaller degree of plasma protein binding of rofecoxib. Thus, [^{11}C]rofecoxib should have suitable characteristics for a PET tracer for monitoring COX-2 expression in the brain. In this study, we found low brain uptake of [^{11}C]rofecoxib (SUV: 0.26±0.09), supposedly reflecting the low expression levels of COX-2 in the brain. In situ hybridization studies have demonstrated that constitutively expressed COX-2 mRNA is not homogeneously distributed in the brain but predominantly located in cortical areas and hippocampus [17,18]. In this study, we showed that the [^{11}C]rofecoxib distribution corresponds with the known distribution of COX-2 mRNA. Moreover, specific binding could be detected in brain regions with constitutive COX-2 expression in blocking studies with the selective COX-2 inhibitor NS398. Binding of NS398 to the active site of the enzyme proved to be a rapid process, as blocking of the binding site was virtually complete within 5 min.

Encouraged by these results, we also evaluated [^{11}C]rofecoxib in a rat model of cerebral inflammation. To this

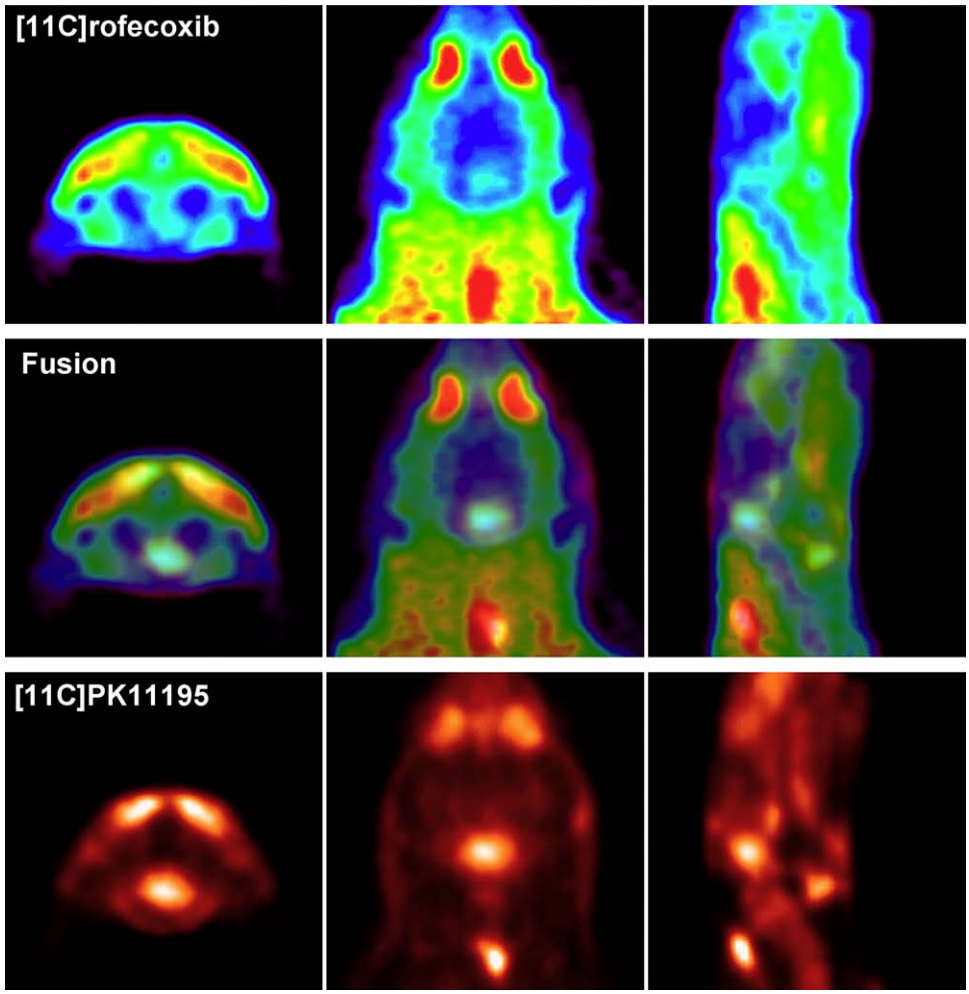

Fig. 3. MicroPET images (0–60 min) of transversal (left), coronal (middle) and sagittal (right) cross sections of the rat brain 7 days after intranasal infection with HSV-1. Rats were anesthetized with a mixture of ketamine (25 mg/kg) and medetomidine (0.2 mg/kg) and injected with approximately 50 MBq of [^{11}C]rofecoxib (upper row) or [^{11}C]PK11195 (bottom row). A coregistration of both images is displayed in the middle row. Increased uptake is observed in the area of the brain stem and cerebellum for both tracers.

purpose, the HSV-induced viral encephalitis model was chosen because the severe inflammatory response that occurs in this model should evoke substantial COX-2 overexpression [2]. After intranasal infection of Wistar rats with HSV, the replicating virus migrates into the brain where it induces intense inflammation. Consequently visible symptoms of illness occur that increase in severity from Day 5 on [16]. These symptoms include stressed behaviour, lethargy, impaired motor function and paralysis. Without treatment, approximately 20% of the animals die within a week after infection. In this model, viral infection of the brain with HSV type 1 was confirmed by reverse transcriptase-polymerase chain reaction analysis of the virus in brain homogenates, immunohistochemistry for activated microglial cells in brain sections and microPET imaging of replicating herpes virus and microglial activation with [^{18}F] FHPG and [^{11}C]PK11195, respectively [16,19]. Despite the presence of severe neuroinflammation, COX-2 overexpression could not be demonstrated with [^{11}C]rofecoxib in this

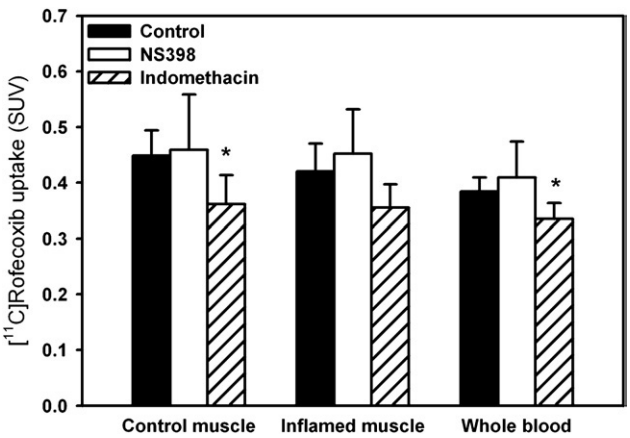

Fig. 4. [^{11}C]Rofecoxib uptake 60 min post injection in control muscle, inflamed muscle and whole blood of Wistar rats that where intramuscularly injected with turpentine 24 h before administration of the tracer. In blocking studies, 1.5 mg/kg NS398 or indomethacin was iv injected 5 min before tracer injection. *Significantly different from controls, as determined by a two-sided unpaired Student's t test ($P<.05$).

model, when a group comparison between infected and control animals was made. Still, brain areas with higher intensity in the [^{11}C]rofecoxib PET images than the surrounding brain that coincided with areas of microglial activation were observed in some animals. This could indicate that the absolute amount of COX-2 overexpression in this model is too low for detection or that the brain penetration or the sensitivity of the tracer is insufficient. Although in principle the amount of COX-2 overexpression in HSV-infected brain could have been determined with, e.g., an peroxidase assay, we decided to abandon this model and to further investigate the feasibility of [^{11}C] rofecoxib for imaging of COX-2 expression in a completely different model instead: a sterile inflammation in peripheral tissue by intramuscular injection of turpentine.

Previously, we have shown that intramuscular turpentine injection results in visible swelling of the inflamed thigh muscle within 24 h due to an acute inflammatory reaction, which can be clearly visualized by flourodeoxyglucose PET [21,22]. Histological examination 24 h after turpentine injection revealed that the inflamed muscle contains partially necrotic muscle fibers that show massive infiltration of neutrophils. At the border of the inflammatory infiltrate, macrophages and fibroblasts were present. Activated neutrophils and macrophages are known to express elevated levels of COX-2 [23,24]. In this model, the tissue distribution of a tracer dose of [^{11}C]rofecoxib (data not shown) was in good agreement with the distribution of [^{14}C]rofecoxib (2 mg/kg iv) in healthy Sprague–Dawley rats, as was described in the literature [14]. This indicates that the PET tracer [^{11}C]rofecoxib displays a similar in vivo behavior as the native drug. Nevertheless, we could not demonstrate any increased [^{11}C]rofecoxib uptake in the inflamed muscle relative to the control muscle. Moreover, tracer uptake in neither muscle could be saturated with the COX-2 inhibitor NS398, whereas a small but significant reduction in tracer uptake was observed after pretreatment with the nonselective COX inhibitor indomethacin. A similar effect was observed in whole blood. Possible explanations could be that [^{11}C]rofecoxib specifically binds to COX-1 in muscle, monocytes and platelets. It has been suggested that selective COX-2 inhibitors also show weak and reversible binding to COX-1 [25]. The high selectivity of some inhibitors for the COX-2 isoform is thought to be due to their ability to irreversible bind to the active site of this isoform. Alternatively, the effect of indomethacin may not be due specific binding to COX-1 but to an indomethacin-induced effect on tracer clearance, resulting in lower tracer concentrations in tissue. A possible explanation for the lack of specific binding could be that the enhancement in tracer uptake as a result of increased COX-2 expression was counteracted by the formation of edema in the muscle, which leads to a reduction in uptake of the lipophilic tracer per gram of tissue. Another possibility could be that the absolute quantities of COX-2 enzyme that were induced in the inflamed muscle were relatively small compared to the level of nonspecific tracer uptake. Consequently, the small portion of specific tracer uptake in the muscle would be completely obscured. To test the latter hypothesis, we performed a COX peroxidase assay [9] and found no increased COX activity in the inflamed muscle (data not shown). However, it should be noted that this peroxidase assay is not very sensitive to small changes in COX-2 expression, as it measures the combined peroxidase activity of COX-1 and COX-2. Nevertheless, the peroxidase assay suggests that the up-regulation of COX-2 in the inflamed muscle is relatively small.

As follows from the above, [^{11}C]rofecoxib was not able to detect any inflammation-induced COX-2 overexpression in two animal models of inflammation, despite the fact that rofecoxib is amongst the most potent and selective COX-2 inhibitors currently available. In fact, none of the radiolabeled COX-2 ligands that have been reported in the literature so far, was able to unambiguously demonstrate specific uptake in a model of inflammation. However, it is still a matter of debate whether this lack of success of labeled COX-2 inhibitors is due to shortcomings of the tracers themselves or the result of inadequate animal models that are used for their evaluation. It has unequivocally been demonstrated that COX-2 expression is up-regulated during inflammation, but absolute measures of the COX-2 expression in inflamed tissue are hard to find, as up-regulation of COX-2 expression is generally presented as a relative value with respect to the control situation. Consequently, a potential pitfall could be that, relative to the control situation, COX-2 expression is highly up-regulated in a specific animal model, but the absolute concentration is still too low to be detected by PET, because of extremely low basal expression of the enzyme. Therefore, validated animal models with quantitative data on COX-2 expression are urgently awaited.

5. Conclusion

COX-2 plays an important role in many physiological processes, and overexpression of this enzyme is observed in a variety of diseases. Therefore, a suitable PET tracer for COX-2 could be a useful tool for mechanistic studies, diagnosis and therapy evaluation. The results of this study show that [^{11}C]rofecoxib uptake in normal brain appears to reflect basal COX-2 expression. However, [^{11}C]rofecoxib could not detect inflammation-induced COX-2 overexpression in two distinct rat models of inflammation, despite the fact that severe inflammation was induced in both models. Thus, either the absolute amounts of COX-2 protein that are expressed during inflammation are too low for detection, which would make COX-2 an unsuitable target for imaging, or the sensitivity of [^{11}C]rofecoxib is insufficient for imaging of COX-2 overexpression after an inflammatory response. In

the latter case, a labeled COX-2 inhibitor with sub-nanomolar affinity may be required.

References

[1] Katori M, Majima M. Cyclooxygenase-2: its rich diversity of roles and possible application of its selective inhibitors. Inflamm Res 2000;49: 367–92.

[2] Tzeng SF, Hsiao HY, Mak OT. Prostaglandins and cyclooxygenases in glial cells during brain inflammation. Curr Drug Targets Inflamm Allergy 2005;4:335–40.

[3] Yermakova A, O'Banion MK. Cyclooxygenases in the central nervous system: implications for treatment of neurological disorders. Curr Pharm Des 2000;6:1755–76.

[4] Learn CA, Mizel SB, McCall CE. mRNA and protein stability regulate the differential expression of pro- and anti-inflammatory genes in endotoxin-tolerant THP-1 cells. J Biol Chem 2000;275:12185–93.

[5] Lukiw WJ, Bazan NG. Cyclooxygenase 2 RNA message abundance, stability, and hypervariability in sporadic Alzheimer neocortex. J Neurosci Res 1997;50:937–45.

[6] De Vries EFJ. Imaging of Cyclooxygenase-2 (COX-2) expression: potential use in diagnosis and drug evaluation. Curr Pharm Des 2006;12:3847–56.

[7] Pairet M, van Ryn J. Experimental models used to investigate the differential inhibition of cyclooxygenase-1 and cyclooxygenase-2 by non-steroidal anti-inflammatory drugs. Inflamm Res 1998;47 (Suppl 2):S93–S101.

[8] McCarthy TJ, Sheriff AU, Graneto MJ, Talley JJ, Welch MJ. Radiosynthesis, in vitro validation, and in vivo evaluation of 18F-labeled COX-1 and COX-2 inhibitors. J Nucl Med 2002;43:117–24.

[9] De Vries EFJ, van Waarde A, Buursma AR, Vaalburg W. Synthesis and in vivo evaluation of ^{18}F-desbromo-DuP-697 as a PET tracer for cyclooxygenase-2 expression. J Nucl Med 2003;44:1700–6.

[10] Majo VJ, Prabhakaran J, Simpson NR, Van Heertum RL, Mann JJ, Kumar JS. A general method for the synthesis of aryl [11C] methylsulfones: potential PET probes for imaging cyclooxygenase-2 expression. Bioorg Med Chem Lett 2005;15:4268–71.

[11] Wust FR, Hohne A, Metz P. Synthesis of 18F-labelled cyclooxygenase-2 (COX-2) inhibitors via Stille reaction with 4-[18F]fluoroiodobenzene as radiotracers for positron emission tomography (PET). Org Biomol Chem 2005;3:503–7.

[12] Prabhakaran J, Majo VJ, Simpson NR, Van Heertum RL, Mann JJ, Kumar JSD. Synthesis of [C-11]celecoxib: a potential PET probe for imaging COX-2 expression. J Label Compd Radiopharm 2005;48: 887–95.

[13] Ahuja N, Singh A, Singh B. Rofecoxib: an update on physicochemical, pharmaceutical, pharmacodynamic and pharmacokinetic aspects. J Pharm Pharmacol 2003;55:859–94.

[14] Halpin RA, Geer LA, Zhang KE, Marks TM, Dean DC, Jones AN, et al. The absorption, distribution, metabolism and excretion of rofecoxib, a potent and selective cyclooxygenase-2 inhibitor, in rats and dogs. Drug Metab Dispos 2000;28:1244–54.

[15] Larsen P, Ulin J, Dahlstrom K, Jensen M. Synthesis of [C-11] iodomethane by iodination of [C-11]methane. Appl Radiat Isot 1997; 48:153–7.

[16] Buursma AR, De Vries EFJ, Garssen J, Kegler D, van Waarde A, Schirm J, et al. [^{18}F]FHPG positron emission tomography for detection of herpes simplex virus (HSV) in experimental HSV encephalitis. J Virol 2005;79:7721–7.

[17] Lacroix S, Rivest S. Effect of acute systemic inflammatory response and cytokines on the transcription of the genes encoding cyclooxygenase enzymes (COX-1 and COX-2) in the rat brain. J Neurochem 1998;70:452–66.

[18] Quan N, Whiteside M, Herkenham M. Cyclooxygenase 2 mRNA expression in rat brain after peripheral injection of lipopolysaccharide. Brain Res 1998;802:189–97.

[19] Doorduin J, De Vries EFJ, Dierckx RA, Klein HC. PET imaging of herpes simplex encephalitis in rats. J Label Compd Radiopharm 2007;50(Suppl 1):S60.

[20] Dembo G, Park SB, Kharasch ED. Central nervous system concentrations of cyclooxygenase-2 inhibitors in humans. Anesthesiology 2005;102:409–15.

[21] Yamada S, Kubota K, Kubota R, Ido T, Tamahashi N. High accumulation of fluorine-18-fluorodeoxyglucose in turpentine-induced inflammatory tissue. J Nucl Med 1995;36:1301–6.

[22] van Waarde A, Cobben DC, Suurmeijer AJ, Maas B, Vaalburg W, De Vries EFJ, et al. Selectivity of 18F-FLT and 18F-FDG for differentiating tumor from inflammation in a rodent model. J Nucl Med 2004;45:695–700.

[23] Kimura T, Iwase M, Kondo G, Watanabe H, Ohashi M, Ito D, et al. Suppressive effect of selective cyclooxygenase-2 inhibitor on cytokine release in human neutrophils. Int Immunopharmacol 2003; 3:1519–28.

[24] Kumagai T, Matsukawa N, Kaneko Y, Kusumi Y, Mitsumata M, Uchida K. A lipid peroxidation-derived inflammatory mediator: identification of 4-hydroxy-2-nonenal as a potential inducer of cyclooxygenase-2 in macrophages. J Biol Chem 2004;279:48389–96.

[25] Copeland RA, Williams JM, Giannaras J, Nurnberg S, Covington M, Pinto D, et al. Mechanism of selective inhibition of the inducible isoform of prostaglandin G/H synthase. Proc Natl Acad Sci U S A 1994;91:11202–6.